Polymer 50 (2009) 2874–2884

Contents lists available at ScienceDirect

Polymer

journal homepage: www.elsevier.com/locate/polymer

Biomimetic apatite coating on P(EMA-*co*-HEA)/SiO_2 hybrid nanocomposites

A. Vallés Lluch [a,*], G. Gallego Ferrer [a,b,c], M. Monleón Pradas [a,b,c]

[a] Center for Biomaterials and Tissue Engineering, Universidad Politécnica de Valencia, Cno. de Vera s/n, 46022 Valencia, Spain
[b] Regenerative Medicine Unit, Centro de Investigación Príncipe Felipe, Av. Autopista del Saler 16, 46013 Valencia, Spain
[c] Networking Research Center on Bioengineering, Biomaterials and Nanomedicine, Valencia, Spain

ARTICLE INFO

Article history:
Received 16 December 2008
Received in revised form
6 April 2009
Accepted 9 April 2009
Available online 21 April 2009

Keywords:
Nanocomposite
Silica
Hydroxyapatite (HAp)

ABSTRACT

P(EMA-*co*-HEA)/SiO_2 nanocomposites with silica contents in the range of 0–30 wt% were prepared by co-polymerization of the organic monomers during the simultaneous sol–gel polymerization of the silica precursor. The ability of the hybrids to form hydroxyapatite (HAp) on their surfaces was tested *in vitro* by soaking the samples in a simulated body fluid (SBF) solution for different times up to 35 days. On the one hand, the composition and morphology of the HAp layer formed were characterized by SEM, EDS, FTIR and XRD; on the other, the exchange of soluble silicates and calcium and phosphate ions, and the structural changes taking place in the nanohybrids when immersed in SBF were analyzed by SEM/EDS. This is, up to our knowledge, the first time the HAp nucleation mechanism has been proposed for organic-silica nanohybrids and correlated with their respective nanostructures. The results revealed that the formation of a HAp coating was in all cases limited by the nucleation induction time, but the mechanism and rate of HAp nucleation were found to be different depending on the nanostructure of the samples, which differs, in turn, with the silica content as a consequence of the differing connectivity of the silica network. The nanohybrids with silica contents in the range of 10–20 wt% proved to be the most suitable for the development of bioactive synthetic scaffolds for bone or other mineralized tissues.

1. Introduction

Biomaterials for hard tissue repair need to be biocompatible, osteoconductive, preferably osteoinductive, and have to exhibit mechanical characteristics close to those of bone or teeth. Since the discovery of 45S5 Bioglass® by Hench in 1971 [1], various kinds of ceramics such as Na_2O–CaO–SiO_2–P_2O_5 glasses, sintered hydroxyapatite (HAp) and glass-ceramics containing apatite or wollastonite are known to bond to living bone [2–6]. The bone-bonding materials, so-called bioactive or surface-active biomaterials, are biocompatible materials that form on their surface a layer of a carbonate-containing hydroxyapatite similar to the bone apatite when implanted in the body, and thus bond to the living bone through this apatite layer. This apatite is a low-crystalline calcium-deficient HAp containing sodium, magnesium, chlorine and carbonate [1,2,6–8].

In 1991, Kokubo [7] developed a simple biomimetic test to reproduce the formation of an apatite layer *ex vivo* and thereby evaluate the bioactivity of a given material. This test has been widely used since then for the study of biomineralization on different types of materials [5,7–14] and their ability to form apatite on their surfaces has been correlated with their *in vivo* bioactivities. This means that the *in vivo* bone-bonding ability of a given material can be predicted from the apatite formation on its surface when subjected to this test. An acellular protein-free simulated body fluid (SBF) with ion concentrations, pH and temperature nearly equal to those of the human blood plasma is employed as the medium for apatite nucleation.

Two important surface chemical changes are involved in the apatite deposition mechanism on bioactive glasses [7,9–12,15–17]: (1) preferential diffusion-controlled extraction of Na^+ and/or Ca^{2+} ions out of the glass by exchange with protons from the solution, and (2) hydration and dissolution of the silica network itself, which is rather slow at physiological pH [18]:

$$2(\equiv Si{-}O^-)Ca^{2+} + 2H^+ \rightarrow 2(\equiv Si{-}OH) + Ca^{2+}$$

$$\equiv Si{-}O{-}Si\equiv + H_2O \rightarrow 2\equiv Si{-}OH$$

The ions exchange results in a pH raise and an increase of the ionic activity product of the apatite in the SBF, which was already saturated with respect to HAp. Degradation of the silica network leads to the formation of ≡Si–OH groups at the glass–solution interface and release of soluble $Si(OH)_4$ into the medium. These ≡Si–OH groups provide favourable sites for nucleation of the apatite, while the increasing number of Ca^{2+} ions accelerates the apatite precipitation from the SBF, which is already saturated with respect to HAp. How

* Corresponding author. Tel.: +34963877277; fax: +34963877276.
E-mail address: avalles@ter.upv.es (A. Vallés Lluch).

0032-3861/$ – see front matter © 2009 Elsevier Ltd. All rights reserved.
doi:10.1016/j.polymer.2009.04.022

the formed silanols induce the apatite formation is not totally clear yet, but it has been speculated that it does not occur directly but through electrostatic interactions leading to the formation of a calcium silicate [15,19]. The pH of the SBF (7.4) is much greater than the isoelectric point of the silica (approximately 2). The formed Si–OH groups at the interface reveal negative charge by dissociation or local distribution of electron density. The glass thereby acquires a negative charge that enhances electrostatic interaction with the positively charged calcium ions in the fluid. This reaction results in the formation of an amorphous calcium silicate comprising a neutral or positive charge [14]. The surface thereby acquires a positive charge by accumulation of calcium ions, and interacts electrostatically with the negatively charged phosphate ions in the SBF, leading to the formation of an amorphous calcium phosphate. Once the apatite nuclei are formed [12,15,16,20], they grow spontaneously by consuming the calcium and phosphate ions from the surrounding body fluid. During this process, the amorphous calcium phosphate incorporates OH^- and CO_3^{2-}, Na^+, K^+ and Mg^{2+} ions from the solution and finally crystallizes into HAp, which is the most stable calcium phosphate in aqueous media.

The ability of a surface to precipitate calcium phosphate from SBF depends on its ability to decrease the activation barriers of the spontaneous precipitation [21,22], via homogeneous nucleation in solution (calcium ion release), or via heterogeneous nucleation on specific surface sites. This suggests that biomineralization can be induced by specific surface functional groups acting as effective sites for heterogeneous nucleation of apatite, even with Ca and P absent from the composition. In fact, aside from Si–OH, different functional groups able to develop negative charge at the blood plasma pH have been found to be effective for calcium phosphate nucleation, *e.g.*, phosphate, carboxy, hydroxy and amine groups [12–14,16,23,24].

In order to improve the mechanical properties of bioactive glasses, several polymers have been combined with bioactive glasses or with HAp in the form of particles or fibres to obtain bioactive composites simulating the composition of natural bone [22,25–29], and porous scaffolds of hybrid composites mimicking natural bone structures have been proposed to serve as a support, reinforce and guide new tissue in-growth and regeneration [30–37]. These bioactive hybrids unite the easy processability, structural control and mechanical properties of the polymers with the bioactive character of the glasses.

In recent years many studies have been devoted to the structure, properties and possible applications of polymer/silica nanocomposites obtained by the polymerization of the organic phase during the simultaneous *in situ* sol–gel polymerization of a silica precursor [38–57]. Nonetheless, the idea of hybridizing biocompatible polymers by this procedure for applications in the mineralized tissue regeneration is quite recent [58–61]. Silica is expected to reinforce mechanically the organic matrix and at the same time confer bioactivity to the nanohybrids through the Si–OH groups available at the surface and those likely formed by dissolution of the silica network.

In this work, a hydrophobic/hydrophilic copolymer of poly(ethyl methacrylate-*co*-hydroxyethyl acrylate), P(EMA-*co*-HEA), in a 70/30 wt%, was employed as organic matrix of silica-based nanocomposites, with silica contents in the range of 0–30 wt%. This organic phase combines the good mechanical properties of the EMA component and hydrophilicity of the HEA needed for a good miscibility of the silica precursor mixture [49], for the transport of oxygen and nutrients and for cells metabolism. The synthesis procedure is described in detail in a previous work, and the nanostructure of the obtained nanohybrids has been studied in detail [62]. In [63], these materials have been characterized on the basis of their physico-chemical, mechanical and surface properties. Here, the apatite forming abilities of the nanohybrids have been evaluated and correlated with their different morphologies, and a hypothesis for the apatite nucleation mechanism is advanced.

2. Materials and methods

2.1. Preparation of samples

Nanocomposites of poly(ethyl methacrylate-*co*-hydroxyethyl acrylate), p(EMA-*co*-HEA), with fixed EMA/HEA weight ratio of 70/30 wt% and with varying proportions of silica, SiO_2: 0, 5, 10, 15, 20 and 30 wt%, were obtained in the form of sheets of 0.8 mm in thickness. Briefly, the procedure consisted in preparing an organic solution of the organic monomers with a 0.5 wt% of ethylene glycol dimethacrylate, EGDMA (98%, Aldrich), as crosslinking agent and a 2 wt% of benzoyl peroxide, BPO (97%, Fluka), as thermal initiator, and an inorganic solution of TEOS with distilled water and hydrochloric acid (37%, Aldrich) in the molar ratio 1:2:0.0185, respectively. After 30 min of separate stirring, both solutions were mixed, stirred for another 30 min and injected into glass moulds. The monomeric mixture was polymerized in an oven at 60 °C for 21 h and post-polymerized at 90 °C for 18 h, rinsed in boiling distilled water/ethanol mixture 50/50 vol% for 24 h to eliminate monomer residues and finally dried in a vacuum desiccator at 80 °C until constant weight. Hereafter, the hybrids will be referred to as Hx, x being the percentage of silica. Poly(ethyl methacrylate), PEMA, and poly(hydroxyethyl acrylate), PHEA, homopolymer samples were prepared following the same polymerization procedure as comparison systems. The samples were cut into disk pieces of 8 mm diameter through which a cotton thread was inserted to hang them immersed in vials for the SBF tests.

2.2. Immersion in SBF

The ability of the different materials to form HAp on their surfaces was tested *in vitro*. Samples of the different compositions were immersed for different times up to 35 days in SBF. In order to obtain the SBF, two solutions were prepared. Solution 1 consisted in 1.599 g of NaCl (Scharlau, 99% pure), 0.045 g of KCl (Scharlau, 99% pure), 0.110 g of $CaCl_2 \cdot 6H_2O$ (Fluka, 99% pure), and 0.061 g of $MgCl_2 \cdot 6H_2O$ (Fluka) in deionized ultra-pure water (Scharlau) up to 100 ml. Solution 2 was prepared by dissolving 0.032 g of $Na_2SO_4 \cdot 10H_2O$ (Fluka), 0.071 g of $NaHCO_3$ (Fluka), and 0.046 g of $K_2HPO_4 \cdot 3H_2O$ (Aldrich, 99% pure) in water up to 100 ml. Both solutions were buffered at pH 7.4, by adding the necessary amounts of aqueous 1 M tris-hydroxymethyl aminomethane, $(CH_2OH)_3CNH_2$ (Aldrich), and 1 M hydrochloric acid, HCl (Aldrich, 37% pure). Then, both solutions were mixed to obtain SBF with the following molar ion concentrations: 142 Na^+, 5.0 K^+, 1.5 Mg^{2+}, 2.5 Ca^{2+}, 148.8 Cl^-, 4.2 HCO_3^-, 1.0 HPO_4^{2-}, 0.5 SO_4^{2-} mM.

The disks were vertically suspended by a cotton thread in closed glass vials filled with SBF. The ratio of geometric surface area of sample to solution volume was 0.12 ml mm^{-2}, slightly higher than that proposed by Kokubo and Takadama [5]. The SBF solution was not renewed during the first 7 days. Afterwards, solutions with twice the ion concentrations of SBF were employed, and the solution was renewed each 2–3 days, so as to provide more favourable conditions for apatite growth (increase in the ionic activity product – IP – of the apatite while maintaining the pH and Ca/P molar ratio [64–66]). Samples were withdrawn from the SBF after 1, 3, 5, 7, 14 and 35 days, gently washed with ultra-pure water, room conditioned and finally dried in a vacuum desiccator at 80 °C.

2.3. Characterization

Scanning Electron Microscopy, SEM, images of the materials surfaces were obtained in a Jeol JSM-6300 microscope, with the samples previously sputter-coated under vacuum with gold, 15 kV of acceleration voltage and 15 mm of distance working. Quantification

of elements was achieved by Electron Dispersive X-ray Spectroscopy, EDS, in the mentioned apparatus, with the samples previously sputter-coated with carbon, 10 kV of acceleration voltage and 15 mm of distance working. Silicon was employed as optimization standard.

Fourier-Transform Infrared FTIR spectra of the surfaces were collected in the attenuated total reflection (ATR) mode between 650 and 4000 cm^{-1} with a Thermo Nicolet Nexus spectrometer operating with a 4 cm^{-1} resolution and averaging 128 scans.

Thin-film X-Ray Diffraction, XRD, spectra of the surfaces were acquired in a Philips PW 1820 diffractometer with CuKα radiation of 1200 W (40 kV, 30 mA) and a scanning step of 1 s per step with an increment of 0.01° over a 2θ range between 10 and 40°.

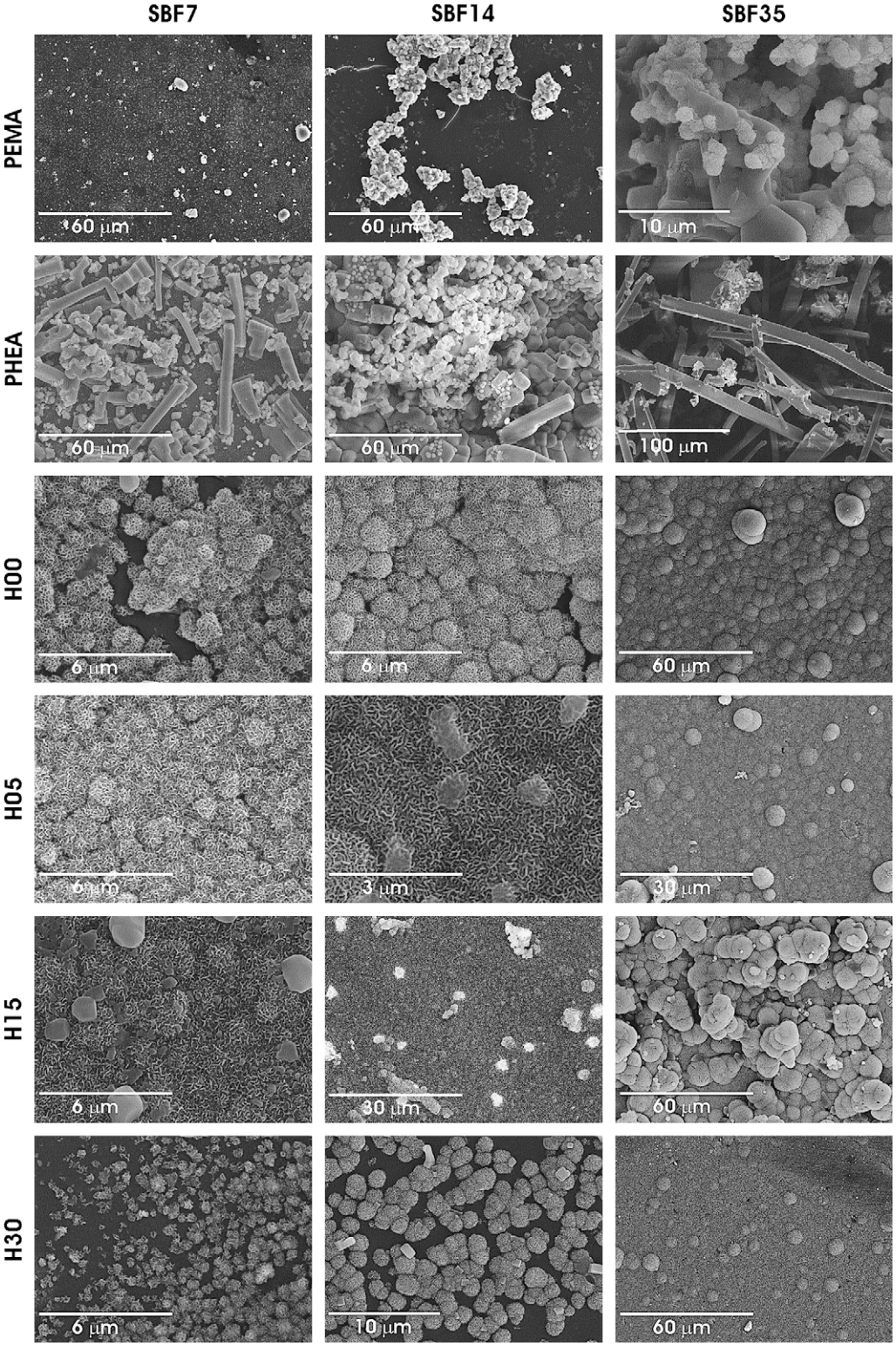

Fig. 1. SEM images of the surfaces of the PEMA, PHEA, H00, H05, H15 and H30 samples after immersion in SBF for different times: 7 days in SBF (SBF7), 7 days in SBF + 7 days in 2 × SBF (SBF14), 7 days in SBF + 28 days in 2 × SBF (SBF35).

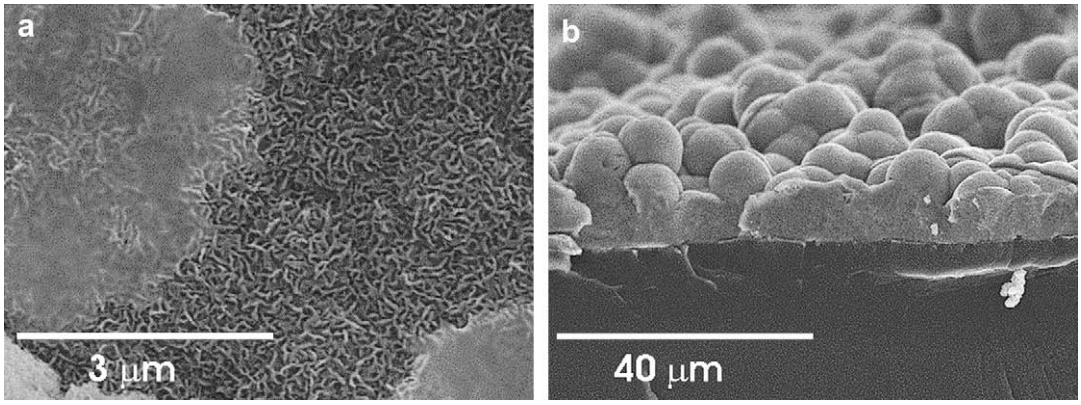

Fig. 2. SEM images of: a) the surface of H10 after 14 days in SBF; b) the transversal fractured section of H15 after 35 days in SBF.

3. Results and discussion

3.1. Characterization of the HAp formed on the substrates in SBF

Fig. 1 shows SEM images of some samples after different times of immersion in SBF. After 7 days (SBF7), the homopolymers PEMA and PHEA did not efficiently induce any apatite growth, while the copolymer did. The PEMA surface nucleates some HAp crystals and precipitates salts from the SBF simultaneously, and the PHEA surface exhibits plenty of precipitates, some of them square or rectangular shaped. The copolymer surface is coated, though imperfectly, with needle-shaped crystals intricately intertwined forming the typical porous cauliflower HAp structures [5,14,64,67] with an average diameter around 1 μm, which merge as they grow to form a continuous uniform coating. The H05 surface is completely coated with these same structures, and the samples H10, H15 and H20 even exhibit superposed scattered aggregates of what seems to be an incipient second layer, and some plain structures anchored to the first coating by needle-like formations. The composition of these uppermost plain structures is the same as that of the cauliflowers below (EDS results not shown). This indicates that the rate of formation of the apatite layer on these hybrids depends on the induction time, but once the apatite nuclei are formed, they grow rapidly. The first apatite layer is composed of porous cauliflowers of nanocrystals with needle or lamellar morphology similar to the apatite structures found in physiological bone. This needle-like

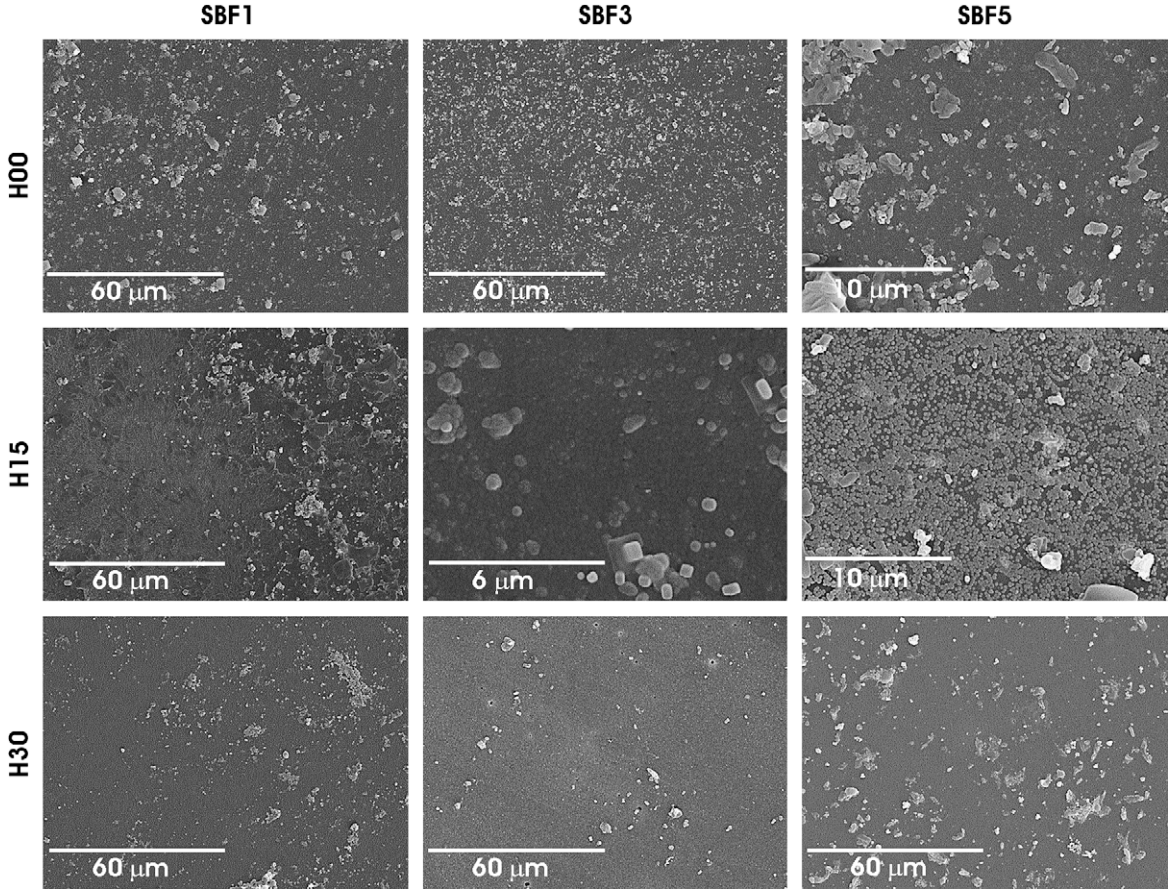

Fig. 3. SEM images of the surfaces of the H00, H15 and H30 samples after immersion in SBF for short times: 1 day (SBF1), 3 days (SBF3), and 5 days (SBF5).

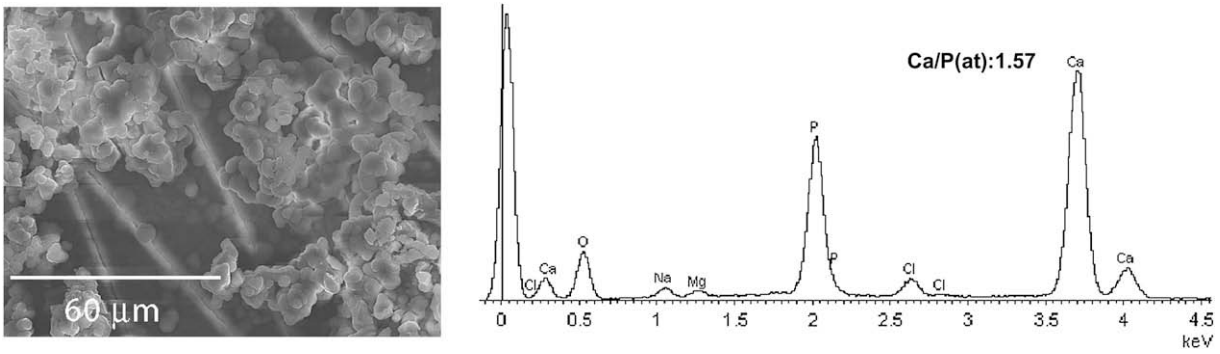

Fig. 4. EDS spectrum of the H20 sample after 35 days in SBF.

morphology has been explained on the basis of the HAp lattice parameters and its symmetry [68], which promote a preferred oriented growth along the *c*-axis. Once apatite has nucleated in a certain location, it grows outwards in a radial pattern [20], leading to cauliflower or hemispherical structures that merge to form a continuous layer. By contrast, only some dispersed smaller cauliflowers appeared on the H30 surface after 7 days, with lower average diameters (around 500 nm), *i.e.*, the copolymer induces the nucleation of HAp crystals, more slowly than the hybrids with 5–20 wt% silica, but faster than H30. This suggests that both polar carboxy and hydroxy groups are effective apatite nucleators, but textural and physical properties such as hydrophilicity and polarity and mechanical modulus of the surface are also relevant.

The body fluid is already supersaturated with respect to the apatite under normal conditions. Once apatite nuclei are formed, they can grow spontaneously by consuming the calcium and phosphate ions from the surrounding body fluid. The 2 × SBF solution, having ion concentrations twice as large as those of SBF, increases the degree of supersaturation of apatite while maintaining the Ca/P atomic ratio. In such a solution apatite is expected to grow more rapidly. The soaking in 2 × SBF (SBF14) promoted the formation of deposits on the surface of PEMA, in combination with typical cauliflower structures. The precipitates without needle-like conformation are salts coming from the SBF, basically NaCl (EDS spectra not shown). PHEA exhibits deposits in several layers, some of them with cauliflower structure, but the majority are rectangular shaped NaCl crystals. As refers to the copolymer, a continuous HAp layer had almost covered its surface after 14 days in SBF (SBF14), and did so completely after 35 days (SBF35).

The HAp cauliflowers of H05, H10, H15 and H20 increased their diameters up to 1–2 µm during the soaking in 2 × SBF, while the flat plates progressively adopted needle-like conformations (Fig. 2a for H10, as an example) and more aggregates of cauliflowers precipitated in successive layers, as shown in the transversal cut of H15 after 35 days in SBF as an example (Fig. 2b). The final thickness of the apatite coating is larger than 10 µm. These four samples display at the end of the test plain areas of merged HAp cauliflowers in combination with others with grape-like aggregates of cauliflowers leading to very irregular topographies. They can be observed for example in the H15 SBF35 image in Fig. 1. This indicates that apatite molecules of the first layer provided secondary nucleation sites for additional apatite formation, which interconnected successive layers [69]. In this stage the amount of nucleating sites at the surface seemed to decrease, and accordingly spherical formations with needle-like nanocrystals grew perpendicularly to the surface leading to the formation of clusters or grape-like structures. This phenomenon has been observed by other authors on starch-based materials [64]. The H30 surface was not completely coated after 14 days in SBF, and it only became completely covered by the end of the test. There was no noticeable difference between the coated hybrids after 35 days of test.

In order to point out the influence of the nature of the substrates on the kinetics of deposition of HAp, the H00, H15 and H30 samples were soaked in SBF for shorter times: 1, 3 and 5 days. The SEM images are shown in Fig. 3. After 1 day, H00 and more markedly H15 presented some dotted zones and scattered salt deposits, whereas H30 exhibited only scattered deposits. After 3 days, in H00 the distribution of nuclei and precipitates was more uniform, the H15 hybrid already showed some areas completely coated with small HAp cauliflowers, whereas only scattered deposits had precipitated on H30. After 5 days, the H15 surface was almost coated with HAp cauliflowers, whereas the H00 presented nuclei and deposits, and H30 revealed only some deposits on the surface, *i.e.*, H30 needed a longer incubation period than the copolymer.

From the EDS and FTIR results, the composition of the HAp coatings was inferred. The results from the EDS spectra of the homopolymers have not been tabulated because the coatings of PHEA consist basically of NaCl, which is the main component of the SBF solution, and the EDS spectra on PEMA differ considerably depending on the analyzed zones, showing Ca and P of HAp in some zones, while NaCl in others. Fig. 4 shows a typical EDS profile of the HAp coating of a hybrid. The main elements are Ca and P, but other elements from the SBF like Na, Mg, K and Cl are also present. The chemical composition of biological apatite is not fixed due to the

Table 1
Ca/P, (Ca + Na + Mg + K)/P, Na/Ca, Mg/Ca atomic ratios of the apatites formed on the hybrids after different times in SBF.

	SBF7				SBF14				SBF35			
	Ca/P	(Ca +Na + Mg + K)/P	Na/Ca	Mg/Ca	Ca/P	(Ca +Na + Mg + K)/P	Na/Ca	Mg/Ca	Ca/P	(Ca +Na + Mg + K)/P	Na/Ca	Mg/Ca
H00	1.34	1.85	0.31	0.07	1.38	1.68	0.16	0.04	1.48	1.73	0.12	0.04
H05	1.47	1.62	0.07	0.04	1.35	1.48	0.05	0.05	1.44	1.61	0.07	0.04
H10	1.26	1.51	0.14	0.05	1.37	1.96	0.20	0.15	1.50	1.75	0.11	0.05
H15	1.48	1.80	0.11	0.07	1.33	1.96	0.34	0.08	1.49	1.68	0.07	0.05
H20	1.53	2.54	0.47	0.16	1.25	1.37	0.03	0.05	1.57	1.79	0.10	0.04
H30	1.58	1.94	0.06	0.00	1.39	1.60	0.11	0.04	1.65	1.87	0.05	0.04

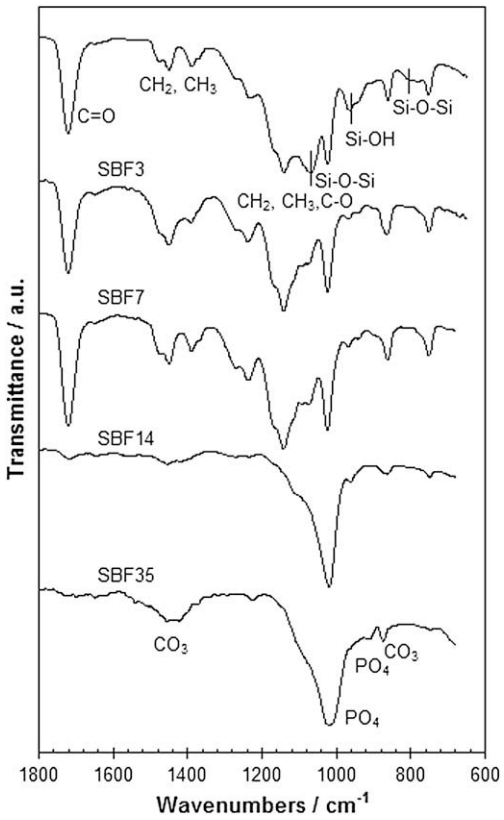

Fig. 5. FTIR spectra of H15 after different times in SBF, in the 600–1800 cm^{-1} region.

different elements available in the body. Among the substituting ions in bone and tooth minerals are Na^+, K^+, Fe^{2+}, Mg^{2+}, F^- and Cl^-, and also complex ions such as CO_3^{2-} and HPO_4^{2-} [65]. Silicon is observed in the EDS spectra after 7 days of immersion in SBF in all nanocomposites, it appears in some spectra after 14 days, but it is not detectable in any hybrid by EDS after 35 days in SBF, meaning that the surfaces of the hybrids are completely coated with HAp and the components of the substrates are not present on the uppermost surfaces. From the EDS results, the Ca/P atomic ratio has been calculated in each case for comparison with that of the stoichiometric HAp ($Ca_{10}(PO_4)_6(OH)_2$), Ca/P = 1.67, or physiological HAp, Ca/P = 1.65 [65], Table 1. In general, the Ca/P ratios are slightly lower than the physiological HAp ratio, but in the range of other amorphous calcium phosphates produced in aqueous solution (1.33–1.5) [20], not following any trend with the silica content. For short times, the Ca/P values are quite heterogeneous, but they seem to increase in all cases, approaching the ratio of physiological HAp with the immersion time. Considering the possibility of Mg^{2+}, Na^+ and K^+, substituting the Ca^{2+} in the apatite [70], the (Ca + Na + Mg + K)/P ratios have been calculated and are also listed in Table 1. Initially, there is a considerable difference between Ca/P and (Ca + Na + Mg + K)/P, Na^+ and Mg^+ being the main contributors. The fact that the Na/Ca and Mg/Ca atomic ratios are very low and do not vary significantly may be attributed to the same Na/Ca and Mg/Ca atomic ratios of the solutions. The Mg/Ca, and Na/Ca atomic ratios of the bone apatite are 0.016, and 0.022, respectively [65]. Longer times of immersion in SBF lead to more homogeneous (Ca + Na + Mg + K)/P results, and closer to those of Ca/P.

Despite the existence of calcium phosphates on the copolymer and nanocomposites after 7 days in SBF demonstrated by EDS, FTIR is not able to reveal the apatite peaks until 14 days of immersion, when a regular spectrum appears. Thus, only the FTIR spectra of H15 after the different times of immersion in SBF have been represented (Fig. 5). The well-defined strong peak at 1700 cm^{-1} corresponding to the C=O bonds of the carboxy groups and the complex spectra between 1500 and 650 cm^{-1} of the copolymer disappear. In the hybrids, the intensity of the peaks appearing at 1060–1100 cm^{-1} attributed to the Si–O–Si stretching vibration, and the peak at 950 cm^{-1} characteristic of the Si–OH stretching vibration of the silica phase [39,45,46,58,60,61,71] decrease with the immersion time in SBF, until FTIR cannot detect the original surface.

After prolonged soaking, the apatite peaks become the only components of the FTIR spectra, as the apatite grows in successive layers and completely covers the surfaces of the samples. The new common spectrum presents a well-pronounced peak at 1020 cm^{-1}, a wide peak at 1430–1470 cm^{-1}, and two minor peaks at 880 and 970 cm^{-1}. The peaks at 1020 and 970 cm^{-1} are attributed to the PO_4^{3-} ion (asymmetric and symmetric stretching), and those at 1430–1470 and 875 cm^{-1} are ascribed to the CO_3^{2-} ion (out of plane and stretching mode) [7,39,58,65,69,72,73], occupying PO_4^{3-} sites in the apatite [65]. This confirms that the apatite formed on the substrates is a carbonate ion-containing apatite. Bone and dentin apatite contain approximately 7 wt% carbonate and tooth enamel about 3.5 wt% [68], but when the HAp is deposited from the SBF, there is less substitution of PO_4^{3-} by CO_3^{2-} in the apatite lattice because the concentration of HCO_3^- in the SBF is lower than that in the blood plasma, and consequently the Ca/P ratio is lower. The incorporation of HPO_4^{2-} groups to the apatite cannot be excluded, since its FTIR characteristic absorption band at 868 cm^{-1} is very close to the CO_3^{2-} band at 880 cm^{-1} and they both could be overlapped. The concentration of HPO_4^{2-} ions increases appreciably with increasing IP [65], so its presence in the apatite coatings seems to be quite probable. The characteristic hydroxy band (3570 cm^{-1}) [74] does not appear in any spectra. This is why the spectra have been represented in the 1800–600 cm^{-1} range in Fig. 7. The absence of the OH characteristic band in the FTIR spectra does not necessarily imply that the apatite formed lacks of OH groups, and can be explained on the basis of the rigidity of the dry samples and consequent imperfect contact with the device, because the OH vibration band from the HEA or the silanol terminal groups was not detected, neither. Besides, the lack of OH^- also could be attributed to the demands of charge balance created by the replacement of one PO_4^{3-} group by one CO_3^{2-} group [13,68,70,73]. Nevertheless, bone apatite does not seem to have a high concentration of OH^- groups, if it contains any OH^- groups at all. Indeed, there is growing evidence for the lack of OH^- in bone apatite [68]. For the PEMA sample, the characteristic apatite spectrum does show up only after 35 days of SBF immersion, and for the PHEA sample it never happens to appear, the spectrum having always HAp absorption bands overlapped with polymeric bands.

Fig. 6 shows the X-ray diffraction patterns of samples H00, H15 and H30 before soaking in SBF and after 14 and 35 days in SBF. After 14 days in SBF, the peaks corresponding to the coatings are poorly resolved and the broad band corresponding to the amorphous hybrid predominates in the three spectra. This correlates well with the Ca/P values. After 35 days, the broad peak at 32–34° and the peak at around 26° attributed to XRD of HAp crystals [9,11,64–66,72,75,76] are well defined. The intensity of these peaks decreases in the order: H15 > H30 > H00. The broad band corresponding to the hybrid in H15 has completely vanished, it is slightly noticeable in H00, but in H30 it maintains the initial shape and overlaps with the HAp peaks. Bone apatite also contains a high amorphous content.

It is well established that HAp formation from metastable aqueous solutions is usually preceded by a precursor phase, most commonly amorphous calcium phosphate (ACP) ($Ca_2(PO_4)_3$) or octacalcium phosphate (OCP) ($Ca_8H_2(PO_4)_6$) [20]. The precursor calcium phosphate then hydrolyzes into the more thermodynamically stable HAp. HAp is the only thermodynamically stable

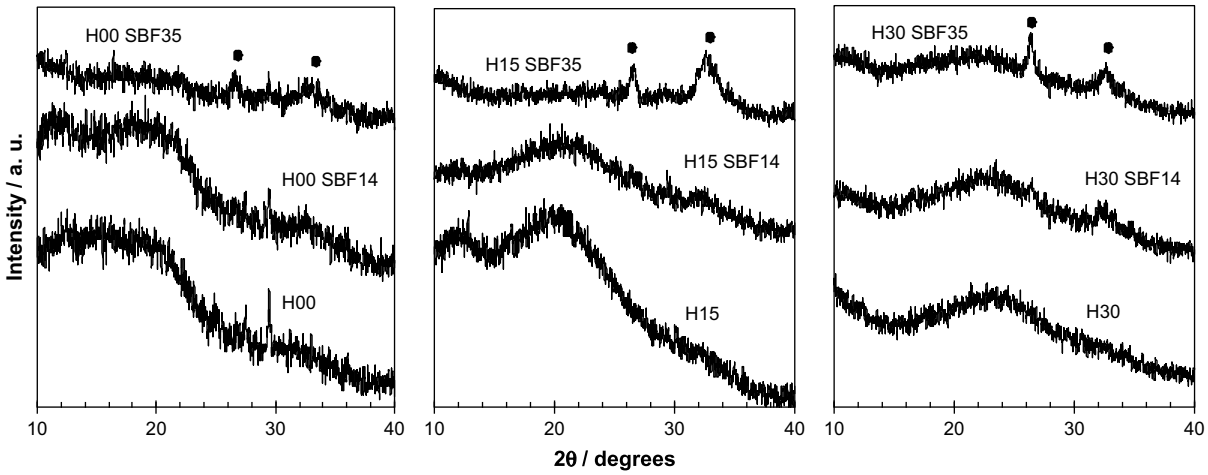

Fig. 6. XRD spectra of H00, H15 and H30 and after 14 and 35 days in SBF.

calcium phosphate that exists in aqueous solution at a pH greater than 4.2 [77].

3.2. Structural changes of the nanohybrids in SBF

In agreement with recent works [13,20,24,64] our results suggest that the carboxy and hydroxy groups of the surface of the copolymer have negative dipoles strong enough so as to interact electrostatically with Ca^{2+} ions from the SBF and form complexes. Phosphate ions may then bond with calcium forming calcium phosphate. The Ca^{2+} ions adsorbed by the copolymer can contribute to the formation of additional nucleating sites. Zainuddin *et al.* [13] observed an extensive apatite deposition in PHEMA hydrogels on the surface and also inside the hydrogel, and

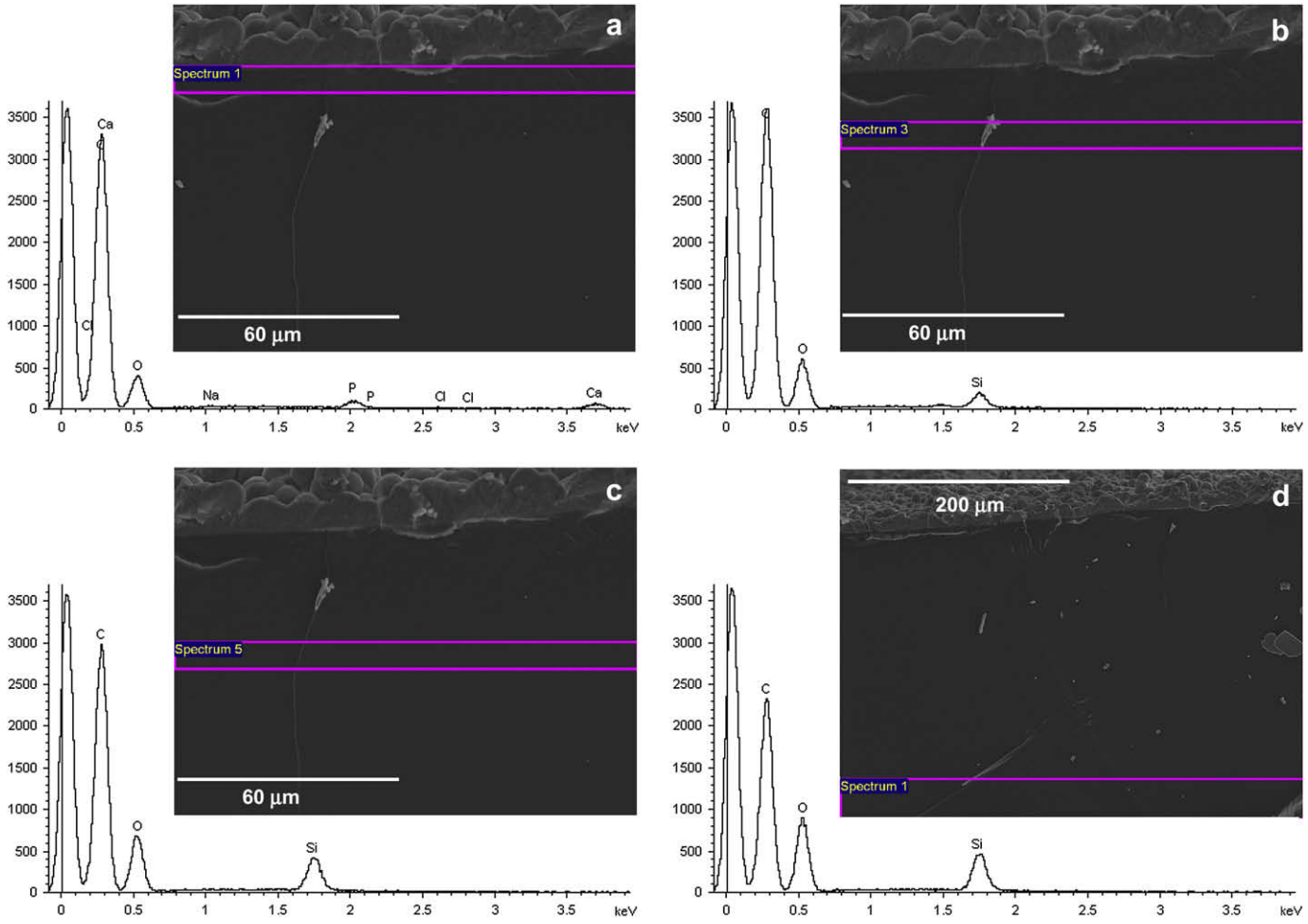

Fig. 7. EDS spectra of different bands in the transversal fractured section of H15 after 35 days in SBF.

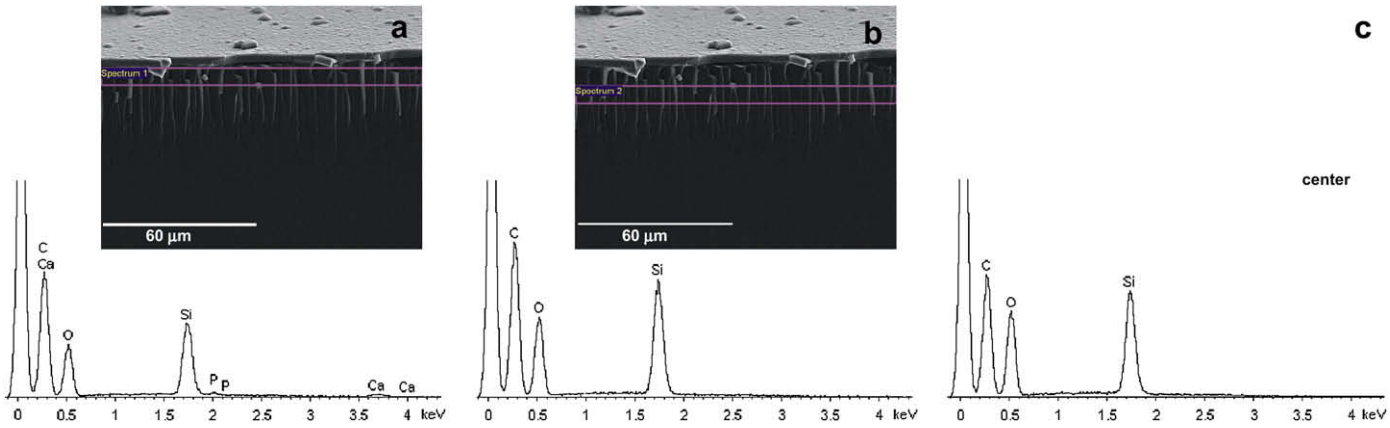

Fig. 8. EDS spectra of different bands in the transversal fractured section of H30 after 35 days in SBF.

attributed it to the presence of functional groups able to chelate Ca^{2+} ions, and to the swelling ability that facilitates the diffusion of ions into the hydrogel.

Silanol groups have higher potential for induction of apatite nucleation than carboxy or hydroxy groups [14]. However, this potentiality does not increase monotonously with the silica content in our samples, but achieves a maximum at an intermediate silica concentration: the rate of apatite precipitation follows the sequence H10, H15, H20 > H05 > H00 > H30. In order to study the structural changes taking place in the hybrids when immersed in SBF and the influence of silica, H15 and H30 samples previously soaked in SBF for 35 days were fractured, and EDS spectra were taken for different successive in-depth bands of the fractured cross-section, each band of approximately 8 μm of thickness, from the HAp–nanohybrid interface towards the interior of the samples. Figs. 7 and 8 display some of the EDS spectra of the fractured H15 SBF35 and H30 SBF35 samples, respectively.

In the H15 hybrids, silica is absent in the first 10 μm-deep layer closest to the surface, then the silica content increases linearly up to 48 μm in depth, where it reaches a value of 14.92 wt%, similar to that found in the middle of the cross-section (13.46 wt%), and those found previously in the original H15 samples on the surface (15.09 wt%) and in the interior (15.33 wt%) by EDS [62]. The correlation of the silica contents calculated from the EDS silicon content of each position relative to the surface has been represented in Fig. 9. Fig. 10 displays some of the EDS spectra obtained by bands in a fractured H15 sample after 35 days in SBF but at higher magnifications and closer to the surface. The spectra demonstrate that silica is nearly absent in the interface (only traces of silica can be detected in some spectra) and that the HAp grows continuously within the material: Ca, P, but also Na, Mg and Cl ions diffuse to the interior of the hybrid (Ca, P, Na, Mg and Cl elements can be detected up to 3.5 μm in depth, the Ca/P ratio being 1.36 up to 3 μm), giving rise to a strongly adhered coating layer.

It seems that fairly strong bonds are formed between the polar groups of the material and the calcium ions of the apatite layer. On the contrary, in the H30 hybrids the silica network does not dissolve. Fig. 9 shows that in the H30 sample after 35 days in SBF, the silica content close to the surface (32.46 wt%) is similar to that in the interior (33.41 wt%), and those found in the original H30 samples on the surface (28.45 wt%) and in the interior (24.87 wt%) by EDS [62]. In this sample the HAp coating is not adhered to the surface as a continuous layer. This different behaviour of the silica networks in the different hybrids affects the nature of the heterogeneous nucleation which occurs during the formation of the first HAp layer, and therefore this layer will be anchored differently to different hybrids.

The different growth modes of the apatite layer can be explained on the basis of the different morphologies of the nanohybrids as a function of the different structure of their silica network. As demonstrated by our previous results [62] and by results on the related PHEA/SiO_2 system [78], in the P(EMA-*co*-HEA)/SiO_2 hybrids the degree of connectivity of the nanosilica network depends on the amount of silica in the sample: for low silica contents the network consists in disconnected nano-domains uniformly dispersed in the organic polymer matrix. The network terminal groups at the surfaces of these domains are noncondensed silanol groups. They increase the polarity of the nanocomposite surface [63]. For higher silica concentrations the inorganic network percolates and becomes a continuous network, interpenetrated with the organic polymer matrix. This percolation threshold seems to be a value around a 15 wt% of silica. Percolation of the silica network is accompanied by a decrease of the free, non-condensed silanol groups on a silica mass unit (Fig. 11), which thus cease to be available at the hybrid surfaces. According to this, the dissolution of the silica network in nanocomposites of subpercolating silica concentrations, such as the H15 sample, is facilitated by the presence of large numbers of silanol terminal groups leading to low-molecular-weight silicates able to diffuse from the hybrid. In this reaction zone of a few μm, calcium and phosphate ions are adsorbed and interact with the polar groups to form calcium phosphates. The apatite growth continues at the interface hybrid-solution leading to a strongly adhered apatite layer. For superpercolating silica concentrations, such as in the sample H30, the continuous and more perfectly packed silica network has fewer noncondensed surface silanol groups, and thus silica dissolution and the Ca^{2+} diffusion are decreased, and therefore the HAp nuclei can only grow from the preexisting nucleating functional groups available at the surface. The bioactivity or HAp nucleating ability of the

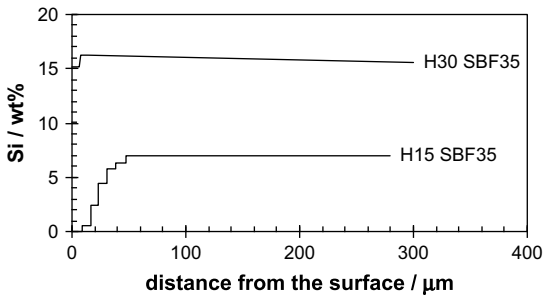

Fig. 9. Correlation of the silica content with the position relative to the surface in H15 and H30 samples after 35 days in SBF.

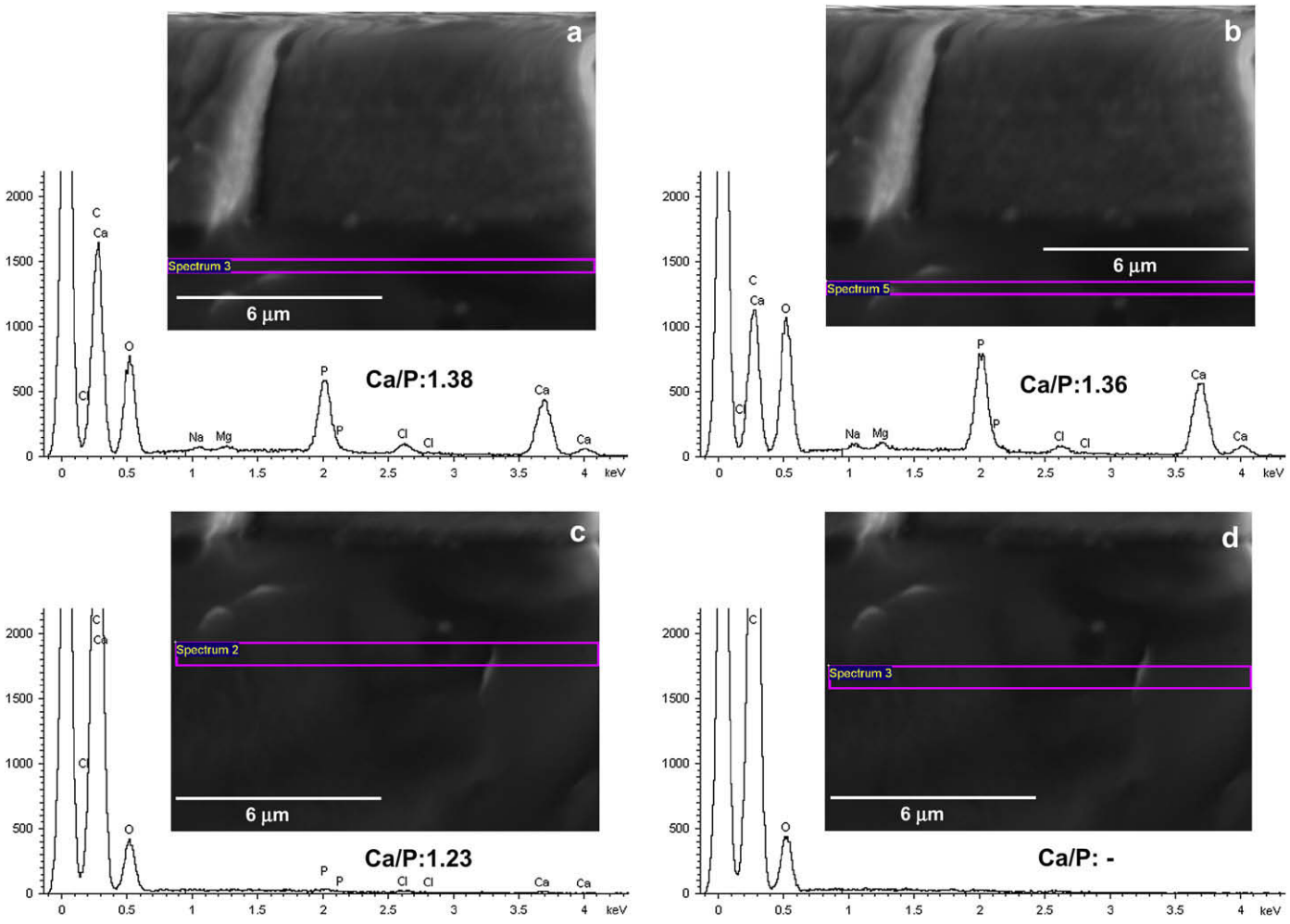

Fig. 10. EDS spectra of different bands in the transversal fractured section of H15 after 35 days in SBF, close to the surface.

H30 hybrid sample thus is even lower than that of the copolymer. This can be explained as a consequence of a lower polarity in the case of the H30 hybrid [63], and of a second factor, which would also explain why the P(EMA-*co*-HEA) copolymer is more bioactive than the pure PEMA homopolymer: the network expansion. The presence of HEA monomer units in the P(EMA-*co*-HEA) copolymer lowers the glass transition temperature and the modulus of the copolymer with respect to those of pure PEMA and, moreover, in an aqueous environment facilitates the network swelling because of its hydrophilic character. This swelling increases the number of polar groups available on a unit area basis by exposing them more efficiently, and facilitates diffusion of the solution ions. This would explain the greater bioactivity of P(EMA-*co*-HEA) 70/30 wt% with respect to PEMA. In the case of the H30 hybrids, the density and tight continuity

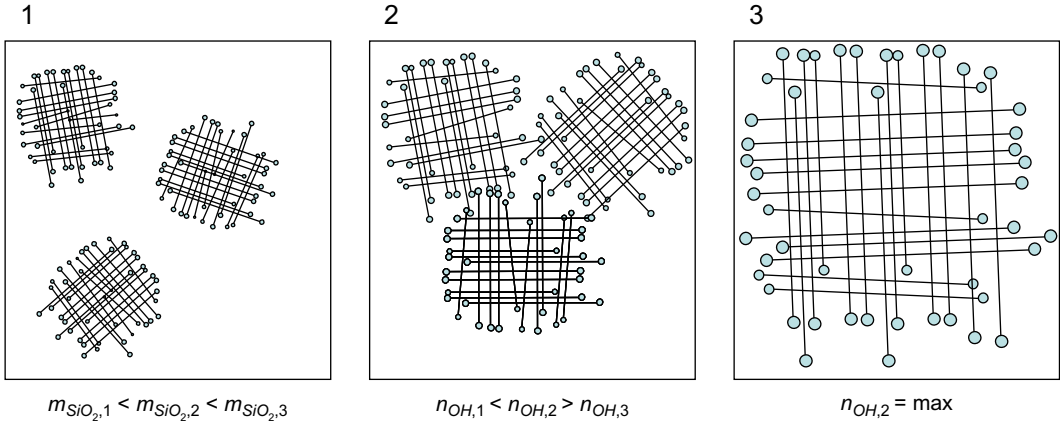

Fig. 11. Sketches of different silica network structures: (1) low concentration subpercolating silica, (2) higher concentration, about to percolate silica, and (3) high concentration superpercolating silica $m_{SiO2,1} < m_{SiO2,2} < m_{SiO2,3}$ $n_{OH,1} < n_{OH,2} > n_{OH,3}$ $n_{OH,2}$=max.

of the silica network completely impedes the polymer network swelling, which is an additional reason why this sample is less bioactive than the copolymer.

4. Conclusions

The bioactivity of hybrids of P(EMA-*co*-HEA) with varying proportions of silica (0–30 wt%) as well as the homopolymers PEMA and PHEA has been investigated in a simulated body fluid with ion concentrations, pH and temperature nearly equal to those of human blood plasma. PEMA and PHEA did not induce the apatite growth efficiently. The copolymer induced the nucleation of apatite crystals, more slowly than the hybrids with 5–20 wt% silica, but faster than that with 30 wt%. This demonstrates that the presence of the carboxy and hydroxy groups has a synergy effect for inducing the apatite nucleation and growth, probably in that it facilitates the network expansion in the aqueous medium leading to an exposure of a larger number of nucleating sites and to enhanced intrapolymer diffusion. Concerning the hybrids, the heterogeneous nucleation to form the first apatite layer depends on the amount of silica and the topology of the silica network. In nanohybrids with intermediate silica contents (10–20 wt%), the dissolution of silica at the surface is facilitated by the presence of large numbers of non-condensed silanol terminal groups in the network and by the disconnected topology of the silica phase; the solution process releases soluble silicates and renders an interface layer rich in silanol groups. In this reaction zone of a few μm calcium and phosphate ions are adsorbed and interact with the polar groups of soluble and hydrated silica to form calcium phosphates. The apatite growth continues at the interface hybrid-solution leading to a strongly adhered apatite layer. After 7 days, the surfaces are completely coated, and even provide secondary nucleation sites for the precipitation of spherical structures with the same needle-like morphology. Above a silica concentration threshold of approximately 20 wt%, the dense and continuously extended silica network hinders the organic polymer network expansion and the diffusion of Ca^{2+} ions, and has a lower density of non-reacted surface silanols, leading to a lesser dissolution of the silica network at the interface, and thus the nucleation of apatite occurs even more slowly than on the copolymer.

Once apatite nuclei have been formed, the growth of the apatite layer and formation of successive layers by homogeneous nucleation occurs very rapidly in all cases, consuming calcium and phosphate ions from the SBF. The initially amorphous calcium phosphate, containing other ions such as CO_3^{2-}, Na^+, K^+ or Mg^{2+}, stabilizes leading to low-crystalline nanocrystallites of calcium-deficient carbonated-hydroxyapatite, with Ca/P ratios near the physiological HAp ratio.

Acknowledgements

The authors thank Dr. Mª Carmen Millán (Departamento de Física, Universidad Politécnica de Valencia) for her help in the XRD measurements. Dr. G. Gallego acknowledges the financial support received from the spanish MEC through the DPI2007-65601-C03-03 project. Dr. M. Monleón acknowledges the financial support received from the INS Carlos III.

References

[1] Hench LL. The story of bioglass. J Mater Sci Mater Med 2006;17:967–78.
[2] Kokubo T. Bioactivity of glasses and glass-ceramics. In: Ducheyne P, Kokubo T, Blitterswijk CA, editors. Bone-bonding biomaterials. Leidendorp: Reed Healthcare Communications; 1992. p. 31–46.
[3] Bajpai PK, Billote WG. In: Bronzino JD, editor. The biomedical engineering handbook. CRC Press, University of Iowa; 1995. p. 552.
[4] Hench LL, Kokubo T. In: Black J, Hastings G, editors. Handbook of biomaterials properties. London: Chapman & Hall; 1998. p. 355.
[5] Kokubo T, Takadama H. How useful is SBF in predicting in vivo bone bioactivity? Biomaterials 2006;27:2907–15.
[6] Ben-Nissan B, Ylänen HO. Bioactive glasses and glass ceramics. In: Akay M, editor. Wiley encyclopedia of biomedical engineering. New Jersey: John Wiley & Sons; 2006. p. 354–66.
[7] Kokubo T. Bioactive glass ceramics: properties and applications. Biomaterials 1991;12:155–63.
[8] Kokubo T. Design of bioactive bone substitutes based on biomineralization process. Mater Sci Eng C 2005;25:97–104.
[9] Ohtsuki C, Kokubo T, Yamamuro T. Mechanism of apatite formation on $CaO–SiO_2–P_2O_5$ glasses in a simulated body fluid. J Non-Cryst Solids 1992;143:84–92.
[10] Li R, Clark AE, Hench LL. An investigation of bioactive glass powders by sol–gel processing. J Appl Biomater 1992;2:231–9.
[11] Salinas AJ, Vallet-Regi M, Izquierdo-Barba I. Biomimetic apatite deposition on calcium silicate gel glasses. J Sol–Gel Sci Tech 2001;21:13–25.
[12] Kim HM, Himeno T, Kokubo T, Nakamura T. Process and kinetics of bonelike apatite formation on sintered hydroxyapatite in a simulated body fluid. Biomaterials 2005;26:4366–73.
[13] Zainuddin, Hill DJT, Whittaker AK, Chirila TV. In-vitro study of the spontaneous calcification of PHEMA-based hydrogels in simulated body fluid. J Mater Sci Mater Med 2006;17:1245–54.
[14] Kawai T, Ohtsuki C, Kamitakahara M, Hosoya K, Tanihara M, Miyazaki T, et al. In vitro apatite formation on polyamide containing groups modified with silanol groups. J Mater Sci Mater Med 2007;18:1037–42.
[15] Takadama H, Kim HM, Kokubo T, Nakamura T. Mechanism of biomineralization of apatite on a sodium silicate glass: TEM-EDX study in vitro. Chem Mater 2001;13:1108–13.
[16] Kim HM, Himeno T, Kawashita M, Kokubo T, Nakamura T. The mechanism of biomineralization of bone-like apatite on synthetic hydroxyapatite: an in vitro assessment. J R Soc Interface 2004;1:17–22.
[17] Vallet-Regí M, Salinas AJ, Arcos D. From the bioactive glasses to the star gels. J Mater Sci Mater Med 2006;17:1011–7.
[18] Devreux F, Barboux P, Filoche M, Sapoval B. A simplified model for glass dissolution in water. J Mater Sci 2001;36:1331–41.
[19] Takadama H, Kim HM, Miyaji F, Kokubo T, Nakamura T. Mechanism of apatite formation induced by silanol groups – TEM observation. J Ceram Soc Jpn 2000;108(2):118–21.
[20] Hutchens SA, Benson RS, Evans BR, O'Neill HM, Rawn CJ. Biomimetic synthesis of calcium-deficient hydroxyapatite in a natural hydrogel. Biomaterials 2006;27:4661–70.
[21] Jaakkola T, Rich J, Tirri T, Närhi T, Jokinen M, Seppälä J, et al. In vitro Ca–P precipitation on biodegradable thermoplastic composite of poly(ε-caprolactone-*co*-DL-lactide) and bioactive glass (S53P4). Biomaterials 2004;25:575–81.
[22] Eglin D, Maalheem S, Livage J, Coradin T. In vitro apatite forming ability of type I collagen hydrogels containing bioactive glass and silica sol–gel particles. J Mater Sci Mater Med 2006;17:161–7.
[23] Oliveira AL, Mano JF, Reis RL. Nature-inspired calcium phosphate coatings: present status and novel advances in the science of mimicry. Curr Opin Solid State Mater 2003;7:309–18.
[24] Zainuddin, Hill DJT, Whittaker AK, Lambert L, Chirila TV. Preferential interactions of calcium ions in poly(2-hydroxyethyl metyhacrylate) hydrogels. J Mater Sci Mater Med 2007;18:1141–9.
[25] Liou SC, Chen SY, Liu DM. Phase development and structural characterization of calcium phosphate ceramics–polyacrylic acid nanocomposites at room temperatures in water–methanol mixtures. J Mater Sci Mater Med 2004;15:1261–6.
[26] Yu S, Hariram KP, Kumar R, Cheang P, Aik KK. In vitro apatite formation and its growth kinetics on hydroxyapatite/polyetheretherketone biocomposites. Biomaterials 2005;26:2343–52.
[27] Fang L, Leng Y, Gao P. Processing of hydroxyapatite reinforced ultrahigh molecular weight polyethylene for biomedical applications. Biomaterials 2005;26:3471–8.
[28] Li Z, Yubao L, Aiping Y, Xuelin P, Xuejiang W, Xiang Z. Preparation and in vitro investigation of chitosan/nano-hydroxyapatite composite used as bone substitute materials. J Mater Sci Mater Med 2005;16:213–9.
[29] Oréfice R, Clark A, West J, Brennan A, Hench L. Processing, properties, and in vitro bioactivity of polysulfone–bioactive glass composites. J Biomed Mater Res 2007;80A:565–80.
[30] Jie W, Yubao L. Tissue engineering scaffold material of nano-apatite crystals and polyamide composite. Eur Polym J 2004;40:509–15.
[31] Eglin D, Ali SAM, Perry CC. Comparative study of the in vitro apatite-forming ability of poly(ε-caprolactone)-silica sol–gels using three osteoconductivity tests (static, dynamic, and alternate soaking process). J Biomed Mater Res 2004;69A:718–27.
[32] Zhao L, Chang J. Preparation and characterization of macroporous chitosan/wollastonite composite scaffolds for tissue engineering. J Mater Sci Mater Med 2004;15:625–9.
[33] Li X, Chang J. Preparation and characterization of bioactive collagen/wollastonite composite scaffolds. J Mater Sci Mater Med 2005;16:361–5.
[34] Day RM, Maquet V, Boccaccini AR, Jérôme R, Forbes A. In vitro and in vivo analysis of macroporous biodegradable poly(D,L-lactide-*co*-glycolide) scaffolds containing bioactive glass. J Biomed Mater Res 2005;75A:778–87.
[35] Meretoja VV, Helminen AO, Korventausta JJ, Haapa-aho V, Seppälä JV, Närhi TO. Crosslinked poly(ε-caprolactone/D,L-lactide)/bioactive glass

composite scaffolds for bone tissue engineering. J Biomed Mater Res 2006;77A:261–8.
[36] Rezwan K, Chen QZ, Blaker JJ, Boccaccini AR. Biodegradable and bioactive porous polymer/inorganic composite scaffolds for bone tissue engineering. Biomaterials 2006;27:3413–31.
[37] Seregin V, Coffer JL. Biomineralization of calcium disilicide in porous polycaprolactone scaffolds. Biomaterials 2006;27:4745–54.
[38] Huang SL, Chin WK, Yang WP. Structural characteristics and properties of silica/poly(2-hydroxyethyl methacrylate) (PHEMA) nanocomposites prepared by mixing colloidal silica or tetraethyloxysilane (TEOS) with PHEMA. Polymer 2005;46:1865–77.
[39] Constantini A, Luciani G, Annunziata G, Silvestri B, Branda F. Swelling properties and bioactivity of silica gel/pHEMA nanocomposites. J Mater Sci Mater Med 2006;17:319–25.
[40] Hajji P, David L, Gerard JF, Pascault JP, Vigier G. Synthesis, structure and morphology of polymer–silica hybrid nanocomposites based on hydroxyethyl methacrylate. J Polym Sci Polym Phys 1999;37:3172–87.
[41] Liu YL, Hsu CY, Hsu KY. Poly(methylmethacrylate)–silica nanocomposites films from surface-functionalized silica nanoparticles. Polymer 2005;46:1851–6.
[42] Tian D, Blacher S, Jerome R. Biodegradable and biocompatible inorganic–organic hybrid materials: 4. Effect of acid content and water content on the incorporation of aliphatic polyesters into silica by the sol–gel process. Polymer 1999;40:951–7.
[43] Catauro M, Raucci MG, De Gaetano F, Buri A, Marotta A, Ambrosio L. Sol–gel synthesis, structure and bioactivity of polycaprolactone/$CaO \cdot SiO_2$ hybrid material. J Mater Sci Mater Med 2004;15:991–5.
[44] Wei Y, Jin D, Yang C, Wei G. A fast convenient method to prepare hybrid sol–gel materials with low volume-shrinkages. J Sol–Gel Sci Technol 1996;7: 191–201.
[45] Lin DJ, Chen CC, Chang CL, Su YC, Cheng LP. Observation of nano-particles in silica/poly(HEMA) hybrid by electron microscopy. J Polym Res 2002;9:115–8.
[46] Costa ROR, Vasconcelos WL. Structural modification of poly(2-hydroxyethyl methacrylate)–silica hybrids utilizing 3-methacryloxypropyltrimethoxysilane. J Non-Cryst Solids 2002;304:84–91.
[47] Schiraldi C, D'Agostino A, Oliva A, Flamma F, De Rosa A, Apicella A, et al. Development of hybrid materials based on hydroxyethylmethacrylate as supports for improving cell adhesion and proliferation. Biomaterials 2004;25:3645–53.
[48] Lin DJ, Chen CC, Su YC, Huang SH, Cheng LP. Preparation of silica-filled poly(2-hydroxymethyl methacrylate) nanocomposites cured by photo-irradiation during the sol–gel process. J Appl Polym Sci 2004;94:1927–35.
[49] Jackson CL, Bauer BJ, Nakatani AI, Barnes JD. Synthesis of hybrid organic–inorganic materials from interpenetrating polymer network chemistry. Chem Mater 1996;8(727):733.
[50] Li C, Wu J, Zhao J, Zhao D, Fan Q. Effect of inorganic phase on polymeric relaxation dynamics in PMMA/silica hybrids studied by dielectric analysis. Eur Polym J 2004;40:1807–14.
[51] Costa ROR, Lameiras FS, Vasconcelos WL. Structural control in poly(butyl acrylate)–silica hybrids by modifying polymer–silica interactions. J Sol–Gel Sci Tech 2003;27:343–54.
[52] Takahashi R, Nakanishi K, Soga N. Aggregation behavior of alkoxide-derived silica in sol–gel process in presence of poly(ethylene oxide). J Sol–Gel Sci Technol 2000;17:7–18.
[53] Malucelli G, Priola A, Sangermano M, Amerio E, Zini E, Fabbri E. Hybrid nanocomposites containing silica and PEO segments: preparation through dual-curing process and characterization. Polymer 2005;46:2872–9.
[54] Zoppi RA, Nunes SP. Hybrids of poly(ethylene oxide-*co*-epichlorhydrin) and silica: phase separation, morphology and thermal properties. Polymer 1998;39:6195–203.
[55] Chen Y, Iroh JO. Synthesis and characterization of polyimide/silica hybrid composites. Chem Mater 1999;11:1218–22.
[56] Sengupta R, Bandyopadhyay A, Sabharwal S, Chaki TK, Bhowmick AK. Polyamide 6,6/in situ silica hybrid nanocomposites by sol–gel technique: synthesis, characterization and properties. Polymer 2005;46:3343–54.
[57] Landry CJT, Coltrain BK, Landry MR, Fitzgerald JJ, Long VK. Poly(vinyl acetate)/silica filled materials: material properties of in situ vs. fumed silica particles. Macromolecules 1993;26:3702–12.
[58] Rhee SH, Choi JY, Kim HM. Preparation of a bioactive and degradable poly(ε-caprolactone)/silica hybrid through a sol–gel method. Biomaterials 2002;23:4915–21.
[59] Rhee SH. Effect of molecular weight of poly(ε-caprolactone) on interpenetrating network structure, apatite-forming ability, and degradability of poly(ε-caprolactone)/silica nano-hybrid materials. Biomaterials 2003;24:1721–7.
[60] Costa ROR, Pereira MM, Lameiras FS, Vaconcelos WL. Apatite formation on poly(2-hydroxyethyl methacrylate)–silica hybrids prepared by sol–gel process. J Mater Sci Mater Med 2005;16:927–32.
[61] Pereira MM, Jones JR, Orefice RL, Hench LL. Preparation of bioactive glass–polyvinyl alcohol hybrid foams by the sol–gel method. J Mater Sci Mater Med 2005; 16:1045–50.
[62] Vallés A, Rodríguez JC, Gallego G, Monleón M. Synthesis and characterization of P(EMA-*co*-HEA)/SiO_2 nanohybrids for mineralized tissue regeneration, Macromolecules, submitted.
[63] Vallés A, Gallego G, Monleón M. Properties of P(EMA-*co*-HEA)/SiO_2 nanohybrids for mineralized tissue regeneration. J Mater Sci Mater Med, submitted.
[64] Oliveira AL, Malafaya PB, Reis RL. Sodium silicate gel as a precursor for the *in vitro* nucleation and growth of a bone-like apatite coating in compact and porous polymeric structures. Biomaterials 2003;24:2575–84.
[65] Kim HM, Kishimoto K, Miyaji F, Kokubo T, Yao T, Suetsugu Y, et al. Composition and structure of the apatite formed on PET substrates in SBF modified with various ionic activity products. J Biomed Mater Res 1999;46:228–35.
[66] Tanahashi M, Yao T, Kokubo T, Minoda M, Miyamoto T, Nakamura T, et al. Apatite coating on organic polymers by a biomimetic process. J Am Ceram Soc 1994;77:2805–8.
[67] Balas F, Kawashita M, Nakamura T, Kokubo T. Formation of bone-like apatite on organic polymers treated with a silane-coupling agent and a titania solution. Biomaterials 2006;27:1704–10.
[68] Wopenka B, Pasteris JD. A mineralogical perspective of the apatite in bone. Mater Sci Eng C 2005;25:131–43.
[69] Zhang K, Yan H, Bell DC, Stein A, Francis LF. Effects of materials parameters on mineralization and degradation of sol–gel bioactive glasses with 3D-ordered macroporous structures. J Biomed Mater Res 2003;66A:860–9.
[70] Spanos N, Misirlis DY, Kanellopoulou DG, Koutsoukos PG. Seeded growth of hydroxyapatite in simulated body fluid. J Mater Sci 2006;41:1805–12.
[71] Bosch P, Del Monte F, Mateo JL, Levy D. Photopolymerization of hydroxyethylmethacrylate in the formation of organic–inorganic hybrid sol–gel matrices. J Polym Sci: Polym Chem 1996;34:3289–96.
[72] Abe Y, Kokubo T, Yamamuro T. Apatite coating on ceramics, metals and polymers utilizing a biological process. J Mater Sci Mater Med 1990;1:233–8.
[73] Siriphannon P, Kameshima Y, Yasumori A, Okada K, Hayashi S. Formation of hydroxyapatite on $CaSiO_3$ powders in simulated body fluid. J Eur Ceram Soc 2002;22:511–20.
[74] Almirall A, Larrecq G, Delgado JA, Martínez S, Planell JA, Ginebra MP. Fabrication of low temperature macroporous hydroxyapatite scaffolds by foaming and hydrolysis of an α-TCP paste. Biomaterials 2004;25:3671–80.
[75] Taguchi T, Muraoka Y, Matsuyama H, Kishida A, Akashi M. Apatite coating on hydrophylic polymer-grafted polyethylene films using an alternate soaking process. Biomaterials 2001;2:53–8.
[76] Oyane A, Uchida M, Choong C, Triffitt J, Jones J, Ito A. Simple surface modification of poly(ε-caprolactone) for apatite deposition from simulated body fluid. Biomaterials 2005;26:2407–13.
[77] Vallet-Regí M, Rodríguez-Lorenzo LM, Salinas AJ. Synthesis and characterization of calcium deficient apatite. Solid State Ionics 1997;101-103: 1279–85.
[78] Rodríguez Hernández JC, Monleón Pradas M, Gómez Ribelles JL. Properties of poly(2-hydroxyethylacrylate)–silica nanocomposites obtained by the sol–gel process. J Non-Cryst Solids 2008;354:1900–8.